Simulation of Current Profile and AC Loss of HTS Winding Wound by Parallel-Connected Tapes

Chen Gu, Timing Qu, Xiaofen Li, and Zhenghe Han

***Abstract*—Field penetration and ac loss of high-temperature superconductor (HTS) windings wound by parallel-connected (PC) tapes are simulated and calculated. The simulation is given to a winding with six tapes, which are connected to produce either $n = 1, 2, 3$, or 6 PC current turns. The PC turns are basically organized as two main types according to whether the turn end is soldered or not. The soldering state is controlled by shunt resistances between HTS tapes. Therefore, six independent PC structures are used for simulation. In addition to the HTS tapes, normal conductors, representing the possible reinforcement layers or stabilizer layers, are also built in the finite-element analysis (FEA) model. The simulation is carried out using the FEA software ANSYS, which is combined with the self-developed resistivity-adaption algorithm, a code that can cope with arbitrary FEA software to simulate field penetration into HTS. More importantly, we used the circuit–field analysis, so that we can adjust n values and the shunt resistance independently while we are simulating the field penetration process. AC loss contributed from different parts of the winding is separately studied as $Q_{\rm HTS}$, which is hysteresis loss generated in HTS; $Q_{\rm nor}$, which is eddy current loss generated in normal conductors; and $Q_{\rm cc}$, which is coupling loss generated in shunt resistances. The current profiles and $Q_{\rm HTS}$ in each tape of the winding are very sensitive to the specific n value. However, the total $Q_{\rm HTS}$ for different PC structures does not significantly change. Even under overestimation, $Q_{\rm nor}$ can only be comparable with $Q_{\rm HTS}$ when the frequency exceeds 1000 Hz. $Q_{\rm cc}$ is prominent at low transport currents but is naturally restrained at high transport currents.**

***Index Terms*—AC loss, field profile, parallel connected (PC), resistivity-adaption algorithm (RAA), simulation.**

I. Introduction

HIGH-TEMPERATURE superconductors (HTS) can tolerate dynamic excitations and, therefore, have potential in electrical devices, which normally work under a 50- to 60-Hz environment [1], [2]. For such dynamic applications, we considered using parallel-connected (PC) HTS tapes to systematically improve the performance of HTS devices. A PC structure, which enhances the critical current in one current bunch, can be used in applications requiring large current, such as resistive-type fault current limiter, transformers, and current leads [3]–[8]. A PC structure also brings more cryogenic stability because minor weak points along HTS tapes can possibly be compensated by sharing current between PC tapes [9]. Moreover, a PC structure can reduce inductance and, thus, can decrease the winding time constant. The decrease in time constant speeds up the charge and discharge of energy in such devices as superconducting magnetic energy storage [10]–[13]. Additionally, a PC structure can be used as a stack to trap fields as an HTS bulk does [14].

However, electromagnetic performance of a winding wound by PC tapes is different from that of a winding wound by a single tape. One of the disadvantages of PC winding is nonuniform current distribution. Nonuniform current distribution is usually analyzed using the electrical circuit method, in which each turn of a winding is regarded as pure inductance [12]. Nonuniform current distribution is caused by the imbalance of inductance between turns. Uniform current distribution can be achieved by balancing the inductance between turns; such balance can be obtained through transposition of turns in a winding [9], [11] or regulation of distance between turns [10].

Recently, Grinenko *et al.* have experimentally tested ac loss of coils wound by PC tapes and theoretically analyzed ac loss in HTS and coupling loss of the coils [15], [16]. However, revealing the loss in each tape and distinguishing the loss from different parts of a winding are experimentally difficult. We therefore usually rely on numerical simulation to deeply understand the loss behavior of a winding in a microstructure. Currently, we can list more than one method that are capable of simulating ac loss of a winding even with hundreds of turns [17]–[20]. However, to our best knowledge, none of those methods can simulate the PC structure because simulating PC structures not only requires applying the current to a specific turn but also regulating the shunt resistance between turns. Recently, the "resistivity-adaption algorithm" (RAA), which is combined with ANSYS, has made simulating PC structures possible [21], [22]. We use the circuit–field function of ANSYS to regulate the parallel connection and meanwhile use the RAA to simulate the field penetration process into HTS.

In this paper, we establish a finite-element analysis (FEA) model composed of HTS tapes, normal conductors surrounding the HTS, and shunt resistances between HTS. The represented winding has six tapes and is assembled by six fundamental PC structures according to the number of tapes in a current bunch and whether the tape end in a current bunch is soldered or not. Hysteresis loss in HTS, i.e., $Q_{\rm HTS}$, with different PC structures is quantitatively calculated and understood with the

Manuscript received May 11, 2013; revised October 11, 2013; accepted November 10, 2013. Date of publication November 20, 2013; date of current version December 7, 2013. This work was supported in part by the National Natural Science Foundation of China under Contract 50907035 and by the Development Foundation for Emerging industries of Shenzhen (JCYJ20130402145002389). This paper was recommended by Associate Editor S. W. Schwenterly.

C. Gu, X. Li, and Z. Han are with the Applied Superconductivity Research Center, Physics Department, Tsinghua University, Beijing 100084, China (e-mail: guchen@tsinghua.edu.cn).

T. Qu is with the Department of Mechanical Engineering, Key Laboratory for Advanced Materials Processing Technology, Tsinghua University, Beijing 100084, China.

Color versions of one or more of the figures in this paper are available online at http://ieeexplore.ieee.org.

Digital Object Identifier 10.1109/TASC.2013.2291276

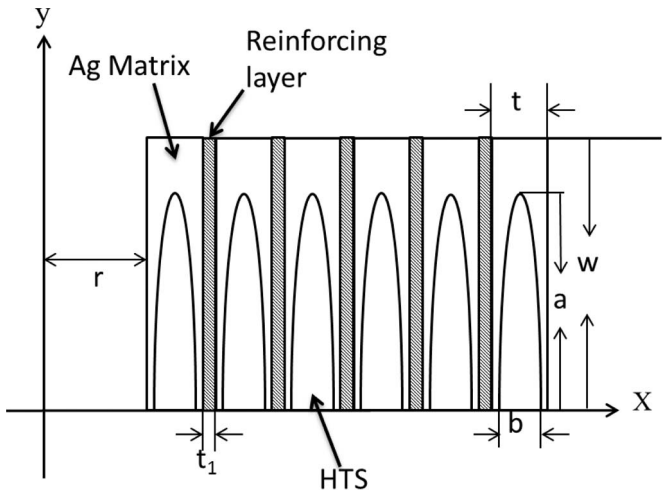

Fig. 1. FEA model for describing the six-tape winding.

TABLE I
GEOMETRICAL PARAMETERS FOR DESCRIBING THE FEA MODEL

Parameters	values
2a	3.878 mm
2b	0.1623 mm
t	0.23 mm
t_1	0.1 mm
2w	4.3 mm
r	0.12 m

help of the current profile in each tape of the winding. Eddy current in normal conductors, i.e., $Q_{\rm nor}$, and coupling loss in shunt resistances, i.e., $Q_{\rm cc}$), are also calculated and compared with $Q_{\rm HTS}$.

II. MODEL FOR SIMULATION

A. FEA Model and Equivalent Circuits for Describing the HTS Winding

As shown in Fig. 1, a six-tape winding is modeled. The winding is a simplification of the vertical legs of a racetrack coil, where only one fourth of the region is modeled because of symmetry. The winding is modeled in a 2-D planar model, by which the tape could be simply regarded as extending a unit length along the z-direction without considering the end effect. All the simulation results in the following sections are given in a unit length. The radius r is set to 0.12 m, large enough in comparison with the winding thickness of 2 mm; thus, fields influenced by the symmetrical winding can be ignored [23]. The HTS part is modeled as an ellipse, which is extracted from the cross section of a Bi2223/Ag multifilamentary (Bi2223) tape. The rectangular cross section surrounding the HTS is assumed to be the silver matrix of a Bi2223 tape. The resistivity of the silver matrix is set to $0.27 \times 10^{-8}\ \Omega \cdot$ m. The rectangular cross section attached with the silver matrix represents the possible mechanical reinforcing layer of a HTS tape [24]. The resistivity of the reinforcing layer is set to $0.19 \times 10^{-8}\ \Omega \cdot$ m. It should be particularly mentioned that the normal conductor layer representing the reinforcing layer is not electrically connected with HTS in the FEA model. However, the silver matrix is electrically connected with the HTS turns. The geometrical parameters of the FEA model are given in Table I.

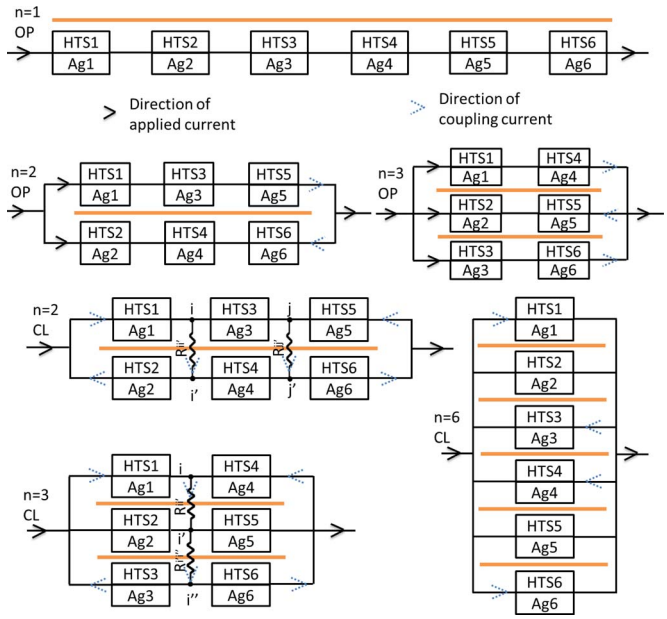

Fig. 2. Equivalent circuits for describing the FEA model. The orange lines that do not electrically connect to the HTS and the silver matrix represent the possible reinforcement layers. Equivalent circuits for describing three tape-open and three tape-close states are denoted as OP and CL, respectively.

The equivalent circuits for describing the FEA model are given in Fig. 2. The six-tape winding is basically assembled by $n = 1, 2, 3, 6$ PC turns. For $n = 2$ and $n = 3$, the equivalent circuit can be separated into two types according to whether the turn ends are soldered (tape-close state) or not (tape-open state). The tapes are soldered only in the end of each turn, and the resistance of the soldered parts is the same for each turn. Thus, shunt resistance is periodically distributed with the same value. In the simulation, the shunt resistances are set to 5×10^2 and $5 \times 10^{-9}\ \Omega$ to represent the tape-open and tape-close states, respectively. According to this turn-end state, $n = 6$ also belongs to the tape-close state, although no shunt resistances are defined between HTS. Therefore, six PC structures are used for simulation: three belonging to the tape-open state and three belonging to the tape-close state. The orange lines that do not electrically connect to the HTS and the silver matrix represent the reinforcement layers.

B. Numerical Simulation of the FEA Model

The simulation is carried out using the FEA software ANSYS [22], which is equipped with the RAA, a self-developed code that can allow any flux motion theory be incorporated into FEA simulation [21], [25]. In this paper, we simply choose the Bean model, i.e., $J_c =$ constant, to describe the HTS. The critical current of a single tape is set to 120 A. Aside from the widely conducted field penetration, one unique feature of this simulation is the combination of circuit analysis and field simulation. Circuit–field analysis enables simple regulation of n values, connection or disconnection of HTS with normal conductors, and introduction of shunt resistances between tapes. The specific way to use circuit–field analysis is given in [21].

The principle of the RAA is based on the fact that the field penetration into HTS can always be simulated by solving

eddy current distribution in a conventional conductor, which is divided into elements that have local resistivity. Therefore, the core of the RAA lies in using an iteration process in identifying the resistivity matrix that can satisfy the E–J relation derived from the flux motion theory in the divided elements [21]. Solving eddy current distribution in conventional conductors is relatively mature and can be achieved by most of electromagnetic FEA packages. By inserting a code to find the resistive matrix, those FEA packages will have the ability to simulate field penetration of HTS. Therefore, the RAA has two advantages: It can collaborate with arbitrary FEA packages that have an eddy current solver, and it can realize arbitrary E–J relations derived from flux motion theory. In this paper, we chose ANSYS because ANSYS can do the "circuit–field" analysis and has the ability to regulate the circuit connection in an easy way. That is one of the reasons we combine the RAA with ANSYS. Next time, when we find other FEA packages that have unique functions we can borrow, we will try to combine the RAA with other FEA packages to facilitate the simulation.

III. Simulation Results

A. Transport AC Loss of HTS

For an HTS that obeys the Bean model, the ac loss could be simply calculated by an integration at I_m, where I_m is the peak current in one cycle [26], i.e.,

$$Q_{\mathrm{HTS}}(I_m) = 4 \int_S J(x,y)\psi(x,y)\, dS \tag{1}$$

where S is the area of the HTS, $J(x,y)$ is the current density, and $\psi(x,y)$ is the flux between an arbitrary point and a kernel in a unit length, i.e., a current-free location. ψ in terms of magnetic vector potential A_z, i.e., the degree of freedom of ANSYS, can be expressed concisely as

$$\psi(x,y) = A_z(x,y) - A_z(x_0,y_0) \tag{2}$$

where $A_z(x_0,y_0)$ is the magnetic vector potential at the kernel. Although (1) is only rigorously valid for a single tape, it is also approximately valid for a pancake coil without strong external perpendicular fields to the surface of the tapes, as discussed in [17], [27], and [28]. The key validness of (1) for a pancake coil is that current fronts must monotonically penetrate from the surface to the insides. Thus, the current distribution for the whole cycle can be obtained from that in the initial stage, which cannot always be done when the tape is simultaneously submitted to an alternating current and applied fields. However, for a pancake coil, although the top and bottom of the tape are exposed to the perpendicular fields, the current front is mostly from the top and bottom of the coil, emulating the behavior of a slab, for which the current fronts do penetrate monotonically.

The Q_{HTS} of a winding obtained by integration at a single state at I_m gives much higher calculation efficiency than the standard method, which should integrate the descendant process from I_m to $-I_m$ by numerous substeps. The time for applying the current from 0 to I_m is set to 0.1 s, quick enough to fully couple the winding if PC structures are adopted. Fig. 3 shows the Q_{HTS} with different n values and with tape-open and tape-close states. I_m and I_c represent the applied current and the critical current in the current bunch, respectively. I_c will double and treble the critical current of a single tape when $n = 2$ and 3, respectively.

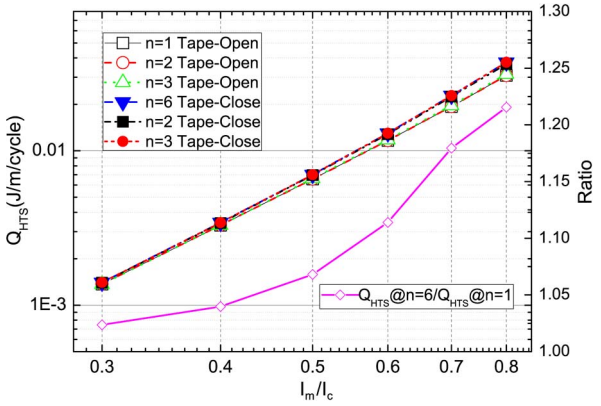

Fig. 3. Total transport ac loss of the six-tape winding as a function of I_m/I_c with different $n = 1, 2, 3, 6$ and with tape-open and tape-close states. The ratio between Q_{HTS} of $n = 6$ and Q_{HTS} of $n = 1$ is also given.

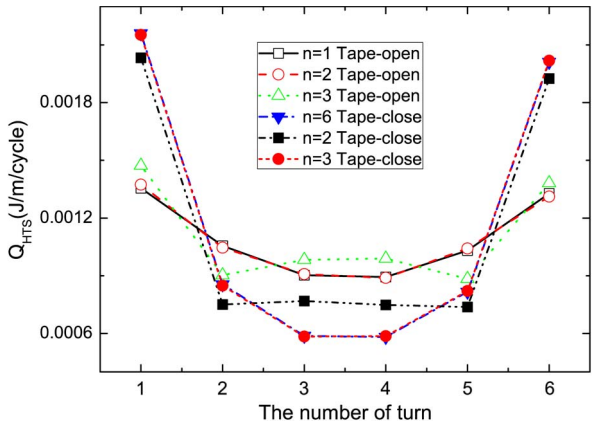

Fig. 4. Transport ac loss distribution along each tape of the winding (from left to right) with different n values and different end states at $I_m/I_c = 0.5$.

Q_{HTS} basically obeys two tendencies according to whether the winding is organized by tape-open or tape-close state. Once the tape-open or tape-close state is determined, Q_{HTS} is not sensitive to the specific n values. In general, Q_{HTS} with tape-close state is larger than that with tape-open state. The divergence becomes increasingly apparent at a high-current region. At a low-current region, the divergence can be ignored.

Furthermore, we observe the ac loss in each tape of the winding with different n values at $I_m/I_c = 0.5$, as shown in Fig. 4. Although r is much larger than the winding thickness, the ac loss in tape 1,2,3 is still slightly larger than in tape 4,5,6 due to fields from the symmetrical winding. In general, regardless of the n value, the outer tapes will have larger ac loss, and the inner tapes will have smaller ac loss. Taking $n = 1$ as a standard, the most uniform loss distribution within tapes produces the smallest Q_{HTS} of the winding as a whole. By contrast, the winding with $n = 6$ has relatively the most nonuniform loss distribution, thereby producing the largest Q_{HTS} of the winding as a whole. The increase in the total Q_{HTS} for tape-close state

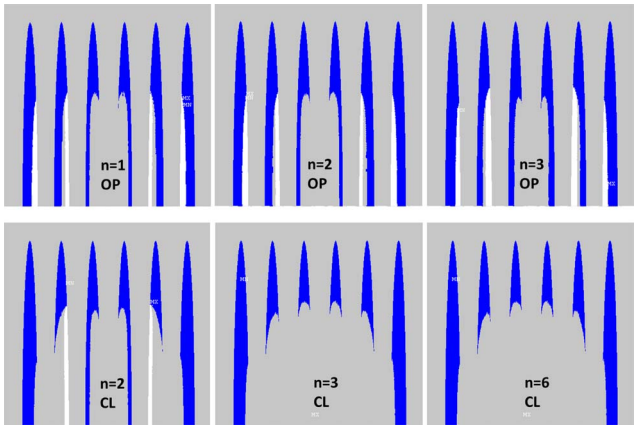

Fig. 5. Current profile in each tape of the winding with different n values and different end states at $I_m/I_c = 0.5$. The top three subfigures are for $n = 1, 2, 3$ and tape-open state. The bottom three subfigures are for $n = 2, 3, 6$ and tape-close state. Blue, white, and gray are for $J = J_c = 2.43 \times 10^8$ A/m^2, $J = -J_c = -2.43 \times 10^8$ A/m^2, and $J = 0$, respectively.

TABLE II
NET CURRENT IN THE EACH TAPE OF THE WINDING FROM THE LEFT TO THE RIGHT. THE CURRENTS ARE GIVEN IN A FULL MODEL

n	End	Turn 1	Turn 2	Turn 3	Turn 4	Turn 5	Turn 6
1	OP	60 A	60 A	60 A	60 A	60 A	60 A
2	OP	61.4 A	58.6 A	61.2 A	58.8 A	61.6 A	58.4 A
3	OP	74.0 A	35.0 A	71.0 A	74.0 A	35.0 A	71.0 A
6	CL	110.4 A	41.6 A	28.0 A	30.0 A	38.8 A	108.2 A
2	CL	109.6 A	10.4 A	61.4 A	59.4 A	12.2 A	107.8 A
3	CL	110.4 A	41.6 A	28.0 A	30.0 A	38.8 A	108.2 A

is acceptable. For example, quantitatively comparing the total $Q_{\rm HTS}$ of $n = 6$ and $n = 1$, at $I_m/I_c = 0.5$, the $Q_{\rm HTS}$ increase is only 6.8%. At $I_m/I_c = 0.9$, the $Q_{\rm HTS}$ increase is no more than 25%. In the tape-close state, the ac loss is intensively focused on the outer tapes, which should be given a particular attention at the design stage. The $Q_{\rm HTS}$ distribution between tapes is further explained by the current profile in Fig. 5. The current profile is supported by the net current data in the tapes from the left to the right, as given in Table II. As expected, different PC structures lead to nonuniform current distributions between tapes, resulting in different $Q_{\rm HTS}$. The more current in the outer tapes, the larger the $Q_{\rm HTS}$ of the winding as a whole. This nonuniform current between tapes is due to a coupling current driven by the time varying of the parallel fields from the neighboring tapes. Therefore, the excitation time, which corresponds to the frequency, is a key factor in determining current distribution and, thus, $Q_{\rm HTS}$. The excitation time of 0.1 s set in the $Q_{\rm HTS}$ calculation is quick enough to reach a high frequency limit, under which the nonuniform current distribution between tapes is in a steady state. However, in Section III-C, we discuss the coupling current and how it affects the current distribution between tapes in a more broad frequency.

When the winding is organized by the tape-open structure, current profiles are fairly similar. In particular, at $n = 1$ and $n = 2$, the current in each tape is almost the same, as quantitatively indicated in Table II. The reason for keeping an identical current distribution is explained in Section III-C, in which the coupling loss is also discussed. At $n = 3$, the middle tapes 2 and 5 show obvious smaller currents than the outer tapes 1 and 6 and the inner tapes 3 and 4. However, the nonuniform current distribution does not result in a significant $Q_{\rm HTS}$ increase in the whole winding (see Fig. 3). The reason is that reduction in the current in tapes 2 and 5 is equally shared by the outer and inner tapes, consequently increasing and decreasing $Q_{\rm HTS}$, respectively.

When the winding is organized by the tape-close structure, the current is exclusively pushed to the outer tapes and behaves as a solid conductor. At $n = 3, 6$, the current profile is almost the same, so does the $Q_{\rm HTS}$ distribution in each tape of the winding.

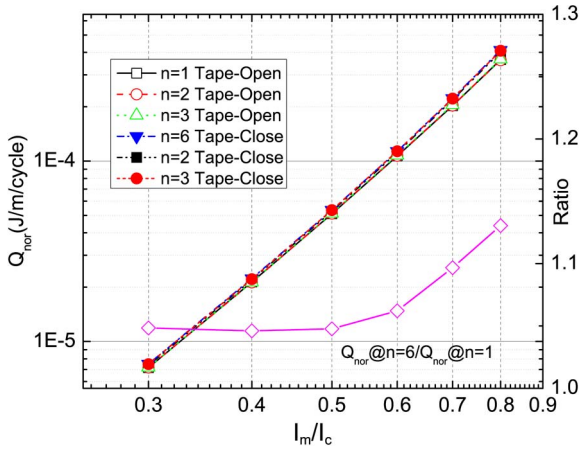

Fig. 6. Total eddy current loss $Q_{\rm nor}$ in the Ag matrix and reinforcement layers as a function of I_m/I_c with different n values. The ratio between $Q_{\rm nor}$ of $n = 6$ and $Q_{\rm nor}$ of $n = 1$ is also given.

B. Eddy Current in Normal Conductors

Eddy current is generated in the normal conductors under ac excitation. The magnitude of eddy current is only a function of excitation rate. Given that the excitation is linear from 0 to I_m, the eddy current should be a constant during the excitation. Eddy current loss per unit length and per cycle is given by the integration of $J \cdot E$ over the whole normal conductor zone at the peak current as

$$Q_{\rm nor} = 4t_0 \int J(x, y; t) E(x, y; t)\, dx\, dy \tag{3}$$

where $J(x, y; t)$ and $E(x, y; t)$ are the current density and the electric field in normal conductors, respectively; and t_0 is the time from 0 to I_m. The total eddy current loss $Q_{\rm nor}$ in the Ag matrix and reinforcement layers as a function of I_m with different n values is given in Fig. 6.

Similar to $Q_{\rm HTS}$, $Q_{\rm nor}$ basically obeys two tendencies according to whether the winding is organized by tape-open or tape-close state. Once the tape-open or tape-close state is determined, $Q_{\rm nor}$ is not sensitive to the specific n values. In general, $Q_{\rm nor}$ with tape-close state is larger than that with tape-open state. The divergence becomes increasingly apparent at a high-current region.

Furthermore, we study $Q_{\rm nor}$ as a function of excitation speed at $n = 6$, as shown in Fig. 7. We apply the current from 0 to a constant value of $I_m/I_c = 0.5$ with different times from the minimum of 0.0001 s, corresponding to a 2500-Hz

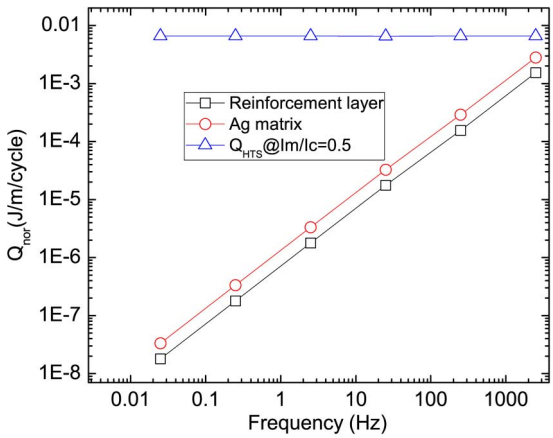

Fig. 7. Eddy current loss in the Ag matrix and reinforcement layers as a function of frequency. For comparison, $Q_{\rm HTS}$ at $I_m/I_c = 0.5$ is also included.

excitation, to the maximum of 10 s, corresponding to a 0.025-Hz excitation. For comparison, the $Q_{\rm HTS}$ at $I_m/I_c = 0.5$ is also included in Fig. 7. Given the amplitude of excitation, $Q_{\rm nor}$ in one cycle is proportional to excitation frequency, whereas $Q_{\rm HTS}$ is independent to excitation frequency. Thus, $Q_{\rm nor}$ is smaller than $Q_{\rm HTS}$ at a low frequency; however, it increases to the level of $Q_{\rm HTS}$ at a high frequency. At a frequency of 50 Hz, $Q_{\rm nor}$ is about two orders of magnitude smaller than $Q_{\rm HTS}$. Even at 250 Hz, a frequency that we are not so often using in electrical applications, $Q_{\rm nor}$ is still about one order of magnitude smaller than $Q_{\rm HTS}$. These finding indicates convergence at the frequency beyond 2000 Hz.

The simulation in this paper is given to a six-tape winding. In a winding with more tapes, the $Q_{\rm HTS}$ and $Q_{\rm nor}$ in a unit length increase at the same speed as the increase in tapes [15], [17]. Therefore, the ignorance of $Q_{\rm nor}$ in comparison with $Q_{\rm HTS}$ in a low frequency is also valid for a real coil with hundreds of tapes.

C. Coupling Loss

Rigorously speaking, the coupling current will be universally generated within a turn and between turns as long as a winding structure is adopted [29], [30]. In this paper, the coupling current is particularly referred as those currents flowing between HTS tapes and not within a single tape. We discuss the coupling current as a separated part not only because it generates loss but also because it is responsible for the nonuniform current distribution between tapes and, thus, the increase in $Q_{\rm HTS}$ of the total winding.

The coupling current is driven by the time-varying parallel fields from the neighboring tapes. If the fields from the symmetrical winding are ignored, then the parallel fields in the winding are antisymmetrically distributed with respect to the center of the winding [15]. Therefore, for $n = 2$ and tape-open state, the net parallel flux enclosed in the whole loop composed of the tapes 1-3-5-6-4-2 is almost zero. Thus, the end-to-end coupling current throughout the winding cannot be obviously found, as shown in Fig. 5. For $n = 3$ and tape-open state, the net flux enclosed in the loops composed of the tapes 1-4-5-2 and 2-5-6-3 is not zero. The net flux arouse the coupling current circling in the two loops, thereby decreasing the current in tapes 2 and 5 and increasing the current in tapes 1 and 4 and tapes 3 and 6 (see Fig. 5 and Table II). For $n = 6$ and tape-close state, the net flux enclosed in any loops composed of the tapes 1-2, 2-3,. . . is not zero. The composition net flux will arouse the coupling current circling in any loops, thereby decreasing the current in the inner turns of 2,3,4, and 5 and increasing the current in the outer turns of 1 and 6. However, the coupling current for the preceding cases, regardless of n value, is only across two terminals, where the resistivity is assumed to be so low that the coupling loss generated at the terminals can be ignored. Therefore, we ignore the discussion of coupling loss for $n = 2, 3$ and tape-open state and for $n = 6$ and tape-close state.

The main discussion of coupling current in this paper is for $n = 2, 3$ and tape-close state, where shunt resistances are periodically defined. The energy dissipated on these shunt resistances is defined as the coupling loss. The shunt resistance in real applications is achieved by soldering the PC tapes along a certain distance. Normally, the longer the soldering zone, the smaller the resistance. For example, 50 nΩ can be easily achieved by soldering a length of 5 cm between two Bi2223 tapes [31]. In the simulation, we first study the coupling current for $n = 2$, where we focus on the coupling current in the loop composed of HTS1, HTS2, and $R_{ii'}$. Assuming that the excitation current from 0 to t_0 is linear, the equation governing the coupling current in the loop can be simply expressed in a typical R-L circuit as

$$L_{\rm eff}\frac{di_{\rm cc}}{dt} + R_{ii'}i_{\rm cc} = M_{\rm eff}\dot{I}_m \tag{4}$$

where $i_{\rm cc}$ is the instantaneous coupling current, and $\dot{I_m}$ is the variation of the transport current of the winding from 0 to I_m. $M_{\rm eff}$ is an effective mutual inductance interacting between the loop and the whole winding. $L_{\rm eff}$ is an effective inductance of the loop. Both $M_{\rm eff}$ and $L_{\rm eff}$ are the most uncertain parts in the equation because they are highly sensitive to the specific penetration state of the HTS. Given that the excitation of I_m is linear, general solution of (4) yields

$$i_{\rm cc} = \frac{M_{\rm eff}I_m\left(1 - e^{-\frac{R_{ii'}}{L_{\rm eff}}t}\right)}{t_0R_{ii'}}. \tag{5}$$

In this equation, $i_{\rm cc}(t_0)$ is denoted by $I_{\rm cc}$.

In Fig. 8, the simulated $I_{\rm cc}$ across $R_{ii'}$ is given as a function of excitation current with different frequencies. Basically, the curves at a small I_m value before I/I_c are rigorously reflected by (5), which is always understood at two extremes. At extremely high frequencies, (5) is reduced to $(M_{\rm eff}/L_{\rm eff})I_m$, with a constant slope dependent on $M_{\rm eff}/L_{\rm eff}$. In a very broad frequency from 2.5 to 250 Hz, the curves are consistent with each other. Therefore, we can attribute 2.5–250 Hz to a high frequency limitation. We can use $I_{\rm cc}/I_m$ to calculate the frequency slope $M_{\rm eff}/L_{\rm eff}$, which fundamentally reflects the tightness between two tapes. Therefore, the largest $M_{\rm eff}/L_{\rm eff}$ cannot exceed 1. At extremely low frequencies, (5) is reduced to $M_{\rm eff}I_m/t_0R_{ii'}$, with variable slopes dependent on frequency.

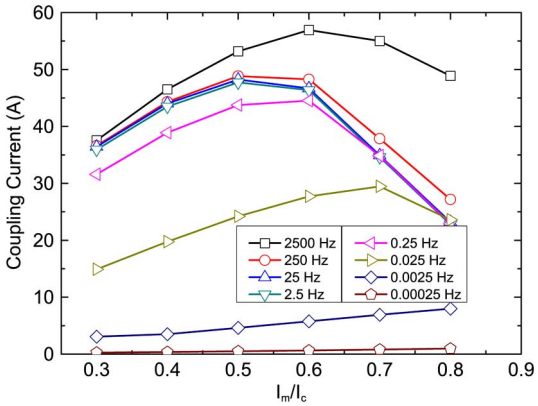

Fig. 8. Coupling current as a function of transport current with different frequencies at $n = 2$ and $R_{ii'} = 25$ nΩ.

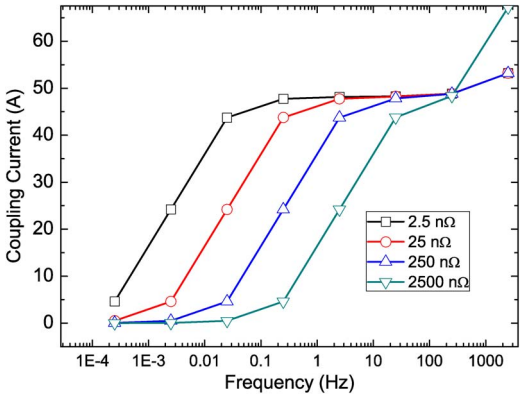

Fig. 9. Coupling current at $I_m/I_c = 0.5$ as a function of frequency with different $R_{ii'}$.

The most intriguing part shown in Fig. 8 is that $I_{cc}(I_m)$ does not monotonically increase with I_m, which apparently breaks the description of (5). In particular, in curves in the high frequency limit, I_{cc} decreases after I_m exceeds 60 A. The reduction in I_{cc} at high transport currents is unique in a winding because the coupling current finally becomes a current in phase with the transport current at the outer turns. The summation of I_{cc} and I_m cannot exceed the critical current of a single tape, e.g., 120 A in this simulation. This feature indicates that the large I_m, after exceeding a certain value, naturally restrains I_{cc} and, thereafter, the coupling loss. At a higher frequency of 2500 Hz, the curves diverge from the high frequency group. We believe that the departure of curve is mainly due to the skin effect, which means that the transport current is shared by the silver matrix at high frequency. Given that the silver matrix shares part of the transport current, the limitation of the total current that cannot exceed 120 A breaks. Therefore, the outer tapes have more room, thereby allowing the coupling current to pass.

To improve understanding, we select the maximum I_{cc} at $I_m/I_c = 0.5$ with different frequencies and add more results with different shunt resistances, as shown in Fig. 9. Regardless of $R_{ii'}$, the maximum I_{cc} reaches a common saturation after the frequency exceeds a certain value. The increase in the shunt resistance results in an entire curve shifting to the high-frequency region. The upturn of the curve at extremely high

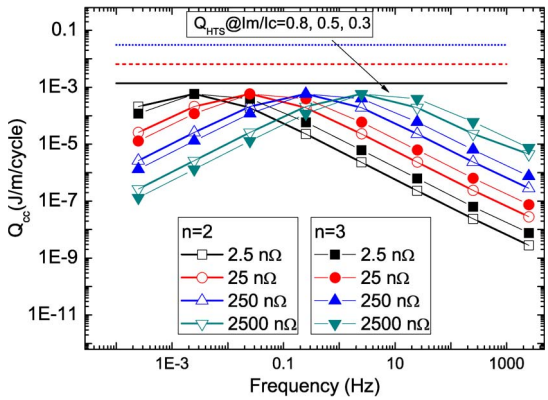

Fig. 10. Coupling loss at $I_m/I_c = 0.5$ as a function of frequency with different $R_{ii'}$. For comparison, three $Q_{\rm HTS}$ curves at $I_m/I_c = 0.3, 0.5,$ and 0.8 are also included.

frequencies is due to skin effect but was not seriously discussed simply because very few HTS electrical devices will work under such high frequency.

AC loss of the coupling current in one cycle and one unit length (Q_{cc}) is approximately obtained by dividing the loss in half at the peak, i.e.,

$$Q_{cc} = \frac{1}{2} I_{cc}^2 R_{ii'} t_0. \tag{6}$$

In Fig. 10, the Q_{cc} at $I_m/I_c = 0.5$ as a function of frequency is plotted. The figure includes both $n = 2$ and $n = 3$ for comparison. The figure is given in a log y scale, so that the "upturn" in the extremely high frequency is not obviously displayed as in Fig. 9. As shown in Fig. 10, no matter how large the value of $R_{ii'}$ is, all curves with different $R_{ii'}$ values reach a common peak with different frequencies. The frequency where Q_{cc} reaches its peak is called the characteristic frequency (CF). The CF moves to a higher region with increasing $R_{ii'}$. From the point where the low frequency limit meets the high frequency limit in (5), we know that the CF is related to the time constant defined by $L_{\rm eff}/R_{ii'}$. Substituting $t_0 = L_{\rm eff}/R_{ii'}$ into (5) yields a constant $I_{cc} = (M_{\rm eff}/L_{\rm eff})I_m(1 - e^{-1})$, which is independent to shunt resistance. From t_0 and (5), we can also roughly estimate $L_{\rm eff}$ and $M_{\rm eff}$ to be 2.5×10^{-7} and 1.6×10^{-7} H, respectively. Moreover, the position of the CF implies that the coupling loss can be reduced by two ways. First, as suggested in [15], HTS devices should be operated away from the CF as much as possible. Second, if the main operation frequency of an HTS device is determined, we can initiatively control the shunt resistance to minimize the coupling loss. At 50–60 Hz, a low shunt resistance of 2.5 nΩ is preferred (see Fig. 10).

In this paper, we use Q_{cc} at $I_m/I_c = 0.5$, the maximum coupling loss, to compare three $Q_{\rm HTS}$ curves at $I_m/I_c = 0.3, 0.5,$ and 0.8. The three $Q_{\rm HTS}$ curves prove that Q_{cc} can only be comparable with $Q_{\rm HTS}$ at small transport current. This conclusion can extend to a winding with hundreds of tapes because the total Q_{cc} is roughly proportional to the square of the tape number, as explained in [32].

Remarkably, the curves for $n = 2, 3$ share a common CF and a common Q_{cc} at a given shunt resistance, although other

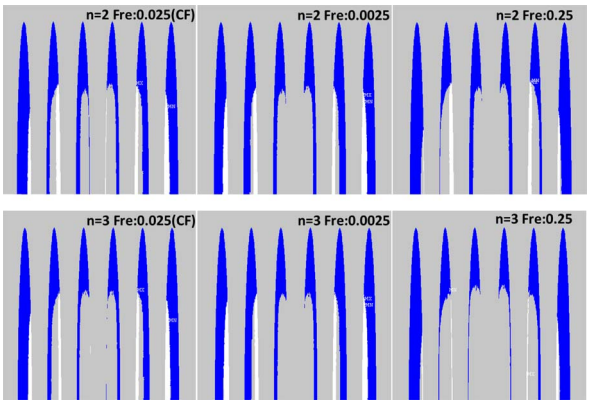

Fig. 11. Current distribution at CF (0.025 Hz) for $I_m/I_c = 0.5$. Blue, white, and gray are for $J = J_c = 2.43 \times 10^8$ A/m^2, $J = -J_c = -2.43 \times 10^8$ A/m^2, and $J = 0$, respectively. For comparison, current distributions of $n = 2$ and 3 at frequencies of 0.0025 and 0.25 Hz are also given.

parts of the curve are inconsistent. The reason for the common CF is that the current distributions for $n = 2, 3$ are identical at this frequency, as shown in Fig. 11. The identical current distributions result in the same $M_{\rm eff}/L_{\rm eff}$ for $n = 2, 3$, which is the root for the common CF. At other frequencies besides the CF, different current distributions for $n = 2, 3$ result in different $M_{\rm eff}/L_{\rm eff}$ and, thus, different coupling losses.

IV. Conclusion

The current profile and ac loss of a six-tape winding wound by PC tapes have been systematically simulated. Using the circuit–field analysis, we can artificially regulate PC structures and, meanwhile, simulate structure-dependent current profile in the winding. AC loss includes $Q_{\rm HTS}$ generated in the HTS, $Q_{\rm nor}$ in the normal conductors surrounding the HTS, and $Q_{\rm cc}$ in the soldering zone between HTS, which are separately studied.

Basically, hysteresis loss is dependent on whether the PC tapes are electrically soldered. When the PC tapes are not electrically soldered, regardless of the number of tapes in a bunch, the total $Q_{\rm HTS}$ of the winding is almost the same. Therefore, we can safely use PC structures to benefit HTS devices without worrying about the increase in ac loss. The total $Q_{\rm HTS}$ is larger in winding with PC tapes electrically soldered than in those not soldered. The increase in $Q_{\rm HTS}$ is due to the nonuniform current distribution between tapes, where intensive current and energy dissipation are focused on the outer turns. The intensive ac loss in the outer turns should be given a particular attention while using PC structures, although the increase in total $Q_{\rm HTS}$ is no more than 10% at $0.5I_c$, which is acceptable in most cases.

Eddy current loss is highly sensitive to the frequency. The $Q_{\rm nor}$ of the six-tape winding is negligibly smaller than $Q_{\rm HTS}$ at the frequency range of 50–60 Hz; however, it increases to the level of $Q_{\rm HTS}$ when the frequency exceeds at least 2500 Hz.

The coupling current is generated as long as PC structures are adopted. It is also the root of nonuniform current distribution between turns. However, $Q_{\rm cc}$ itself is only considerable when the transport current is low and will be naturally restrained when the transport current is large. Over the frequency domain, $Q_{\rm cc}$ reaches the maximum at the CF, which is related to the time constant. From the operation point of view, we should avoid using HTS devices under such CF. From the design point of view, we should initiatively regulate the shunt resistances to leave the CF as much as necessary.

Acknowledgment

The authors would like to thank Dr. D.-X. Chen for helpful discussion.

References

[1] P. Tixador, "Development of superconducting power devices in Europe," *Phys. C*, vol. 470, no. 20, pp. 971–979, Nov. 2010.

[2] G. M. Zhang, S. T. Dai, N. H. Song, Z. Zhu, J. Zhang, W. Guo, D. Zhang, Z. Zhang, L. Xiao, and L. Lin, "The construction progress of a high-Tc superconducting power substation in China," *IEEE Trans. Appl. Supercond.*, vol. 21, no. 3, pp. 2824–2847, Jun. 2011.

[3] A. Hobl, W. Goldacker, B. Dutoit, L. Martini, A. Petermann, and P. Tixador, "Design and production of the ECCOFLOW resistive fault current limiter," *IEEE Trans. Appl. Supercond.*, vol. 23, no. 3, p. 5601804, Jun. 2013.

[4] E. F. Pleva, V. Mehrotra, and S. W. Schwenterly, "Conductor requirements for high-temperature superconducting utility power transformers," *Supercond. Sci. Technol.*, vol. 23, no. 1, p. 014025, Jan. 2010.

[5] A. Berger, S. Cherevatskiy, M. Noe, and T. Leibfried, "Comparison of the efficiency of superconducting and conventional transformers," *J. Phys., Conf. Series*, vol. 234, p. 032004, 2010.

[6] S. W. Lee, H. J. Lee, G. Cha, and J. K. Lee, "Comparison of ac losses of HTS pancake winding with single tape and multi-stacked tape," *IEEE Trans. Appl. Supercond.*, vol. 15, no. 2, pp. 1603–1606, Jun. 2005.

[7] S. Lee, S. Byun, W. Kim, K. Choi, and H. Lee, "AC loss analysis of a HTS coil with parallel superconducting tapes of unbalanced current distribution," *Phys. C*, vol. 463–465, pp. 1271–1275, Oct. 2007.

[8] R. Heller, W. H. Fietz, R. Lietzow, V. L. Tanna, A. Vostner, R. Wesche, and G. R. Zahn, "70 kA high temperature superconductor current lead operation at 80 K," *IEEE Trans Appl Supercond.*, vol. 16, no. 2, pp. 823–826, Jun. 2006.

[9] H. Ueda, A. Ishiyama, K. Shikimachi, N. Hirano, and S. Nagaya, "Stability and protection of coils wound with YBCO bundle conductor," *IEEE Trans. Appl. Supercond.*, vol. 20, no. 3, pp. 1320–1323, Jun. 2010.

[10] T. Hamajima, N. Atomura, Y. Chiba, T. Yagai, M. Tsuda, K. Shikimachi, N. Hirano, and S. Nagaya, "Analysis of current distribution in multi-laminated HTS tape conductor for double pancake coil of SMES," *IEEE Trans. Appl. Supercond.*, vol. 21, no. 3, pp. 1371–1374, Jun. 2011.

[11] N. Atomura, T. Takahashi, Y. Chiba, M. Tsuda, T. Hamajima, K. Shikimachi, N. Hirano, and S. Nagaya, "Homogeneous current distribution experiment in a multi-laminated HTS tape conductor for a double-pancake coil of SMES," *Phys. C*, vol. 471, no. 21/22, pp. 1395–1398, Nov. 2011.

[12] T. Hamajima, N. Harada, M. Tsuda, T. Yazawa, and T. Kuriyama, "Analysis of current distributions in a multi-laminated HTS tape conductor for solenoid coils," *Cryogenics*, vol. 44, no. 5, pp. 341–348, May 2004.

[13] A. Badel, P. Tixador, K. Berger, and M. Deleglise, "Design and preliminary tests of a twin coil HTS SMES for pulse power operation," *Supercond. Sci. Technol.*, vol. 24, no. 5, p. 055010, May 2011.

[14] A. Patel, S. C. Hopkins, and B. A. Glowacki, "Trapped fields up to 2 T in a 12 mm square stack of commercial superconducting tape using pulsed field magnetization," *Supercond. Sci. Technol.*, vol. 26, no. 3, p. 032001, Mar. 2013.

[15] V. Grinenko, G. Fuchs, K. Nenkov, C. Stiehler, M. Vojenciak, T. Reis, B. Oswald, and B. Holzapfel, "Transport ac losses of YBCO pancake coils wound from parallel connected tapes," *Supercond. Sci. Technol.*, vol. 25, no. 7, p. 075006, Jul. 2012.

[16] V. Grinenko1, G. Fuchs, K. Nenkov, and B. Holzapfel, "An efficient method for ac loss reduction of YBCO pancake coils wound from parallel tapes," *Supercond. Sci. Technol.*, vol. 26, no. 3, p. 035002, Mar. 2013.

[17] E. Pardo, "Modeling of coated conductor pancake coils with a large number of turns," *Supercond. Sci. Technol.*, vol. 21, no. 6, p. 065014, Jun. 2008.

[18] E. Pardo, "Calculation of ac loss in coated conductor coils with a large number of turns," *Supercond. Sci. Technol.*, vol. 26, no. 10, p. 105017, Oct. 2013.

[19] Z. Hong, W. Yuan, M. Ainslie, Y. Yan, R. Pei, and T. A. Coombs, "AC losses of superconducting racetrack coil in various magnetic conditions," *IEEE Trans. Appl. Supercond.*, vol. 21, no. 3, pp. 2466–2469, Jun. 2011.
[20] R. Brambilla, F. Grilli, D. N. Nguyen, L. Martini, and F. Sirois, "AC losses in thin superconductors: The integral equation method applied to stacks and windings," *Supercond. Sci. Technol.*, vol. 22, no. 7, p. 075018, Jul. 2009.
[21] C. Gu, T. M. Qu, X. F. Li, and Z. Han, "AC losses in HTS tapes and devices with transport current solved through the resistivity adaption algorithm," *IEEE Trans. Appl. Supercond.*, vol. 23, no. 2, p. 8201708, Apr. 2013.
[22] ANSYS Multiphysics Release 11, ANSYS Inc. [Online]. Available: www.ANSYS.com
[23] H. Kamijo, H. Hata, Y. Fukumoto, A. Tomioka, T. Bohno, H. Yamada, N. Ayai, K. Yamasaki, T. Kato, and M. Iwakuma, "Development of low ac loss windings for superconducting traction transformer," in *Proc. J. Phys., Conf. Series*, 2010, vol. 234, p. 032027.
[24] N. Ayai, S. Kobayashi, M. Kikuchi, T. Ishidaa, J. Fujikamia, K. Yamazakia, S. Yamadea, K. Tatamidania, K. Hayashia, K. Satoa, H. Kitaguchib, H. Kumakurab, K. Osamurac, J. Shimoyamad, H. Kamijyoe, and Y. Fukumoto, "Progress in performance of DI-BSCCO family," *Phys. C*, vol. 468, no. 15–20, pp. 1747–1752, Sep. 2008.
[25] C. Gu and Z. Han, "Calculation of ac losses in HTS tape with FEA program ANSYS," *IEEE Trans. Appl. Supercond.*, vol. 15, no. 2, pp. 2859–2862, Jun. 2005.
[26] W. T. Norris, "Calculation of hysteresis losses in hard superconductors carrying ac: Isolated conductors and edges of thin sheets," *J. Phys. D, Appl. Phys.*, vol. 3, no. 4, pp. 489–507, Apr. 1970.
[27] J. R. Clem, J. H. Claassen, and Y. Mawatari, "AC losses in a finite Z stack using an anisotropic homogeneous-medium approximation," *Supercond. Sci. Technol.*, vol. 20, no. 12, pp. 1130–1139, Dec. 2007.
[28] M. P. Oomen, R. Nanke, and M. Leghissa, "Modelling and measurement of ac loss in BSCCO/Ag-tape windings," *Supercond. Sci. Technol.*, vol. 16, no. 3, pp. 339–354, Mar. 2003.
[29] M. N. Wilson, *Superconducting Magnets*. New York, NY, USA: Oxford Univ. Press, 1983, pp. 174–177.
[30] A. M. Campbell, "A general treatment of losses in multifilamentary superconductors," *Cryogenics*, vol. 22, no. 1, pp. 3–16, Jan. 1982.
[31] C. Gu, C. Zhuang, T. M. Qu, and Z. Han, "Voltage–current property of two HTS tapes connected by ordinary Sn–Pb solder," *Phys. C*, vol. 426-431, pp. 1385–1389, Oct. 2005.
[32] W. J. Carr, Jr., "Loss in a striated coated conductor," *Supercond. Sci. Technol.*, vol. 20, no. 3, pp. 168–175, Mar. 2007.

Chen Gu received the B.Eng. degree from the University of Electronic Science and Technology of China, Chengdu, China, in 2000.

Since July 2000, he has been a Research Engineer with the Applied Superconductivity Research Center, Physics Department, Tsinghua University, Beijing, China. His main research interests include modeling of electromagnetic property of high-temperature superconducting (HTS) tape and devices and design and conceptual construction of new HTS electrical devices.

Timing Qu received the B.Eng. degree in materials science and engineering and the Ph.D. degree in physics from Tsinghua University, Beijing, China, in 2002 and 2007, respectively.

From 2004 to 2005, he was an Exchange Student with Université de Genève, Geneva, Switzerland. In 2007, he began his Postdoctoral Research in the Department of Mechanical Engineering, Tsinghua University, where he acquired a faculty position in 2009 and is currently an Associate Professor. His main research interests include the development of high-temperature superconducting (HTS) tapes and new HTS devices for large-scale applications.

Xiaofen Li received the B.S. degree from Tsinghua University, Beijing, China, in 2006, the M.S. degree from Tsinghua University, and the Ph.D. degree from the Technical University of Denmark, Lyngby, Denmark, in 2011.

He is currently a Research Assistant with the Applied Superconductivity Research Center, Department of Physics, Tsinghua University. His main research interests include electromagnetic properties of superconductors, pinning properties of hard superconductors, and deposition of high-temperature superconducting thin-film materials.

Zhenghe Han received the B.S. degree from Tsinghua University, Beijing, China, in 1982 and the Ph.D. degree from the University of Copenhagen, Copenhagen, Denmark, in 1996.

He is currently the Director of the Applied Superconductivity Research Center, Tsinghua University. He is internationally accepted as the representative of the community of researchers working on the superconducting materials development in China.